IEEE Access
Multidisciplinary | Rapid Review | Open Access Journal

Received October 29, 2020, accepted December 1, 2020, date of publication December 7, 2020,
date of current version December 21, 2020.

Digital Object Identifier 10.1109/ACCESS.2020.3042880

Dual Connectivity in Decoupled Aerial HetNets With Reverse Frequency Allocation and Clustered Jamming

MOHAMMAD ARIF[1], SHURJEEL WYNE[1], (Senior Member, IEEE), KEIVAN NAVAIE[2], (Senior Member, IEEE), MUHAMMAD SAJID HAROON[3], (Graduate Student Member, IEEE), AND SADIA QURESHI[4]

[1]Department of Electrical and Computer Engineering, COMSATS University Islamabad (CUI), Islamabad 45550, Pakistan
[2]School of Computing and Communications, Lancaster University, Lancaster LA1 4WA, U.K.
[3]Telecommunications and Networking (TeleCoN) Research Laboratory, GIK Institute of Engineering Sciences and Technology, Topi 23640, Pakistan
[4]School of Data and Electrical Engineering, University of Technology Sydney, Ultimo, NSW 2007, Australia

Corresponding author: Mohammad Arif (mohammadarif911@gmail.com)

This work was supported in part by the EU-funded project ATOM-690750 under call H2020-MSCA-RISE-2015 and in part by the UK Engineering and Physical Sciences Research Council (EPSRC) under Grant EP/S009620/1.

ABSTRACT The extensive increase in the number of mobile devices and their data-rate requirements will lead to the scarcity of network resources. One of the promising solutions to keep up with the capacity and coverage demands of the 5th generation and beyond of cellular networks is to exploit the dual connectivity (DC) feature in heterogeneous networks (HetNets). In this work, a two-tier aerial HetNet with decoupled access and reverse frequency allocation strategy is considered and the DC feature for the network edge users is investigated. The analytical expressions of the coverage probability for the first and second uplink (UL) connections in DC are derived. Our proposed setup improves the coverage performance of the DC with decoupled access in relation to single connectivity (SC) with and without decoupled access. The results show a relative increase in the DC-based coverage performance of 10.6% and 82.6%, for a signal-to-interference-ratio (SIR) threshold of -20 dB, with respect to SC with and without decoupled access, respectively. Moreover, DC-based coverage in aerial HetNets is resilient to jamming interference. The results also show that if the wide-band jammers (WBJs) are present around a target-user equipment, the legitimate UL transmission is severely disrupted by the jamming interference. For instance, the percentage-decrease in the coverage performance of DC with decoupled access for the SIR threshold set to -20 dB is 4.9% and 10.6%, when the WBJs is set to 2 and 4, respectively. The coverage performance further decreases with an increase in the transmit powers of the WBJs and their number, whereas increases with an increase in the radius of the WBJs cluster.

INDEX TERMS Aerial HetNets, unmanned aerial vehicles, dual connectivity, downlink and uplink decoupling, wide-band jammers.

I. INTRODUCTION

The tremendous increase in the user-demand for capacity and coverage along with the performance improvements due to the proliferation in the scale of mobile devices, services, and wireless networks will lead to scarcity of resources in the 5th generation and beyond of cellular networks. It is anticipated that by the year 2030, the number of machine-type users will reach 97 bn while the number of mobile subscriptions will reach 17.1 bn [1]. This ultra-massive increase cannot be addressed solely by terrestrial networks [2]. The evolution of base stations from terrestrial-fixed to aerial-vehicular is one of the promising solution to maintain the quality of service in such ultra-dense wireless networks [3]–[5]. The aerial heterogeneous networks (HetNets) can enhance the network coverage, efficiently utilize bandwidth resources, create favorable channel conditions, and meet the high capacity demands during concerts, earthquakes, and large sports event [6], [7].

The associate editor coordinating the review of this manuscript and approving it for publication was Giovanni Pau.

The aerial HetNets ensure reliable connectivity and coverage in cases where the line-of-sight (LoS) link is present between the unmanned aerial vehicles (UAVs) and the user equipment (UE) [8], [9]. The UAVs are categorized as high-altitude platforms (HAPs) and low-altitude platforms (LAPs) based on their operating altitude, size, transmission power, battery constraints, endurance capability, and weight [6], [7], [10]. Typically, the UAV-base stations with larger size, endurance-capability, and transmit power are known as HAPs while, the UAVs with less weight, size, and transmission power are considered as LAPs. In [11], the performance of a target-UE (T-UE) is analyzed by assuming various pathloss exponents for the aerial HetNets and it has been shown that the performance of the aerial HetNets is improved, if an LoS link to the T-UE exists.

To further improve the performance of cellular networks, the dual connectivity (DC) paradigm has been proposed to enhance reliable connectivity, capacity, and coverage of the aerial HetNets [12]–[14]. In DC, the UEs are allowed to maintain more than one connection with the UAVs in uplink (UL) and downlink (DL). In [15], [16], it was shown that the performance of a T-UE improves by employing the DC strategy when comparing with the traditional single connectivity (SC) in terms of the coverage probability. Similarly, in [17], [18], the authors showed that the HetNets-performance is significantly improved in terms of the user-throughput if DC is adopted.

Decoupled access is adopted in aerial HetNets to further improve the network's performance [6], [7]. In the decoupled access or the DL and UL decoupling (DUDe), a T-UE is allowed to associate to two different tiers. For instance, in the DL, a T-UE is allowed to be associated with a HAP while, associated with a LAP in the UL, if the decoupled access is permitted. In [19]–[21], it was shown that under the decoupled access, the coverage performance is significantly better when comparing to the without the decoupled access.

The performance of the aerial HetNets can also be improved, if the bandwidth resources are efficiently utilized using reverse frequency allocation (RFA) [7]. In the RFA scheme, the HAPs and LAPs are allowed to operate at the same set of frequencies in UL and DL but in a reverse manner and with sufficient geographical separation (see Sec. II-E). In [22]–[25], it was shown that the coverage performance of HetNets that employ the RFA technique is better than that of similar networks without RFA.

Nevertheless, the HetNets-performance is affected adversely due to the jammers because they can disrupt the legitimate UL communication [26]–[28]. The target-locations of the jammers are airports, train stations, shopping centers, public- and military-gatherings. In such locations, the jammers are grouped in clusters around the target. Typically, the power of the T-UE is very high as compared to the jammers. Therefore, various jammers are used in the cluster to create a jamming attack at the T-UE in order to degrade the legitimate UL communication. The authors in [7], [25] assumed wide-band jammers (WBJs) to consider the impact of jamming due to low-power nodes in aerial HetNets. The nature of WBJs is spatially clustered around a T-UE to exploit the legitimate communication of a T-UE by introducing jamming interference. The jammers can be modeled in aerial HetNets according to a Matern cluster process (MCP) [7], [24], [25]. The number of jamming clusters in an MCP is a random process with Poisson distribution while the number of jammers in a cluster are uniformly-distributed in that cluster (see Sec. III-C2).

Under decoupled access, the aerial HetNets-performance is investigated in conjunction with RFA and WBJs in [7]. Whereas, the DC strategy is investigated in [12], [13], [16]. However, the works are limited in the sense that they do not provide insight into the joint deployment of DC with decoupled access in aerial HetNets that employ RFA in the presence of WBJs. To the best of the authors' knowledge, this is the first research effort to analyze the effect of DC and decoupled access for the aerial HetNets in conjunction with RFA and clustered-jammers. This work is different from the state-of-the-art in the following aspects.

- In [11], the outage probability is investigated for aerial HetNets by assuming multiple pathloss exponents of a K-tier aerial HetNet. However, the research lacks the DC feature in conjunction with RFA and jamming interference.
- In [29], coverage analysis of cellular networks is investigated along with the decoupled access, RFA, and WBJs. Further, in [15], [16], the DC feature for the cellular networks is analyzed. In contrast to these works, we also investigate aerial HetNets.
- In [24], [25], [29], authors assumed the same pathloss exponents to analyze RFA and jamming interference for multiple tiers of HetNets which is considered unrealistic and an oversimplified-approach. However, our analysis considers different pathloss exponents for multiple-tiers in aerial HetNets.
- In [6], the coverage probability analysis of the aerial HetNets employing decoupled access is presented. Further, in [7], decoupled access for the aerial HetNets in the presence of RFA and jamming interference is investigated. However, the research in [6], [7] is limited in terms of the joint analysis of DC and decoupled access. In contrast to these works, we employ DC along with the decoupled access in the presence of RFA and jamming interference.

A. MAIN CONTRIBUTIONS

This work is different from our previous works in [6], [7] in the following aspects. In [6], we derived the association probabilities of a typical UE for different use-cases of aerial-terrestrial HetNets and then derived closed-form expressions for the coverage probability, spectral efficiency, and energy efficiency. Then in [7], we shift the focus of our analysis on the clustered-jamming in aerial HetNets in the presence of RFA and derived analytical expression of the coverage probability of a typical UE in aerial HetNets.

In this work, and in contrast to the aforementioned works, we analyze the DC feature for the edge users of aerial HetNets and derive the coverage probabilities of the first and second UL connection in the presence of RFA by comparing our results with the SC mode. We further investigated the effect of clustered jamming on the edge users in the DC mode. The main contributions which have not been presented in the previous works whatsoever are as the following:

- We investigate the first and second UL connection in DC mode for the edge users of aerial HetNets.
- The analytical expression of the coverage probability is derived for the first and second UL connection in DC mode in the presence of RFA strategy.
- We showed that the WBJs can create jamming interference that causes coverage holes if located in the proximity of a T-UE. We then analyze WBJ's interference on the performance of the aerial HetNets that employ DC functionality.
- We further evaluate the performance of a T-UE employing DC functionality against the WBJ's transmission power, the LAP-associated T-UE's transmission power, the LAP's transmission power, and the WBJ's cluster radius.

B. PAPER ORGANIZATION

The rest of the paper is structured as follows. The system model for a two-tier aerial HetNet in conjunction with the DC feature, decoupled access, RFA, and clustered WBJs is given in Section II. Section III describes the association probability of the decoupled-enabled edge users, density function, and interference at the serving UAVs. Section IV describes the analysis of the DC feature in conjunction with the decoupled access and the SC with and without decoupled access. Then, in Section V we discuss the results and finally, this paper is concluded in Section VI.

II. SYSTEM MODEL

In this paper, we extend our previous-work [6], [7] by focusing on the DC functionality for the aerial HetNets in the presence of decoupled access, RFA, and WBJs.

A. DEPLOYMENT OF INFRASTRUCTURE

We model aerial HetNet with two tiers in the presence of RFA and WBJs (see Fig. 1). The deployment scenarios along with the transmission powers of UAVs, UEs, and WBJs are presented in the next subsections.

1) UAVs DEPLOYMENT

We assume that the HAPs and LAPs in the aerial HetNets are distributed according to the independent homogeneous Poisson point process (HPPP), Φ_H, and Φ_L, respectively [30], [31]. The density of HAPs and LAPs is set to λ_H and λ_L, respectively whereas, the transmit power of the HAPs and LAPs is set to P_H and P_L, respectively. Moreover, the HAPs and LAPs are assumed to be hovering at the height of h_H and h_L, respectively.

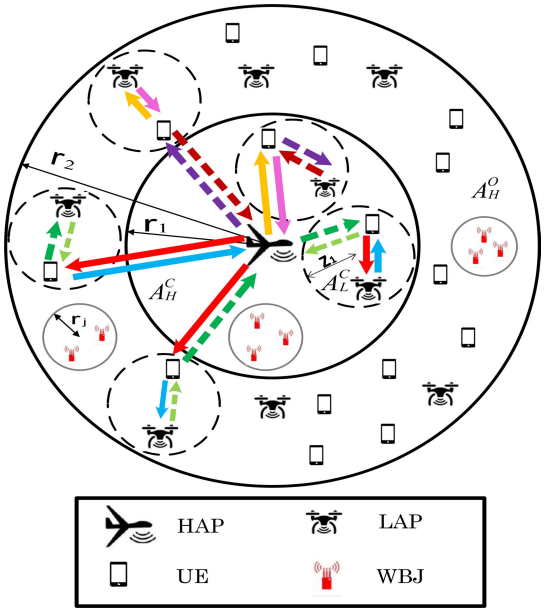

FIGURE 1. System model for a two-tier aerial HetNet. The solid lines show the first connection and the dotted lines show the second connection. Different colored lines are in accordance with the color scheme in RFA (see Sec. II-E).

2) UEs DEPLOYMENT

The UEs are distributed according to independent HPPPs, Φ_U, with the density of UEs set to λ_U. The UEs are assumed to be located at the ground and the transmit power of the UEs associated with HAP and LAP is set to Q_H and Q_L, respectively. The serving UE is referred to as a T-UE and is placed at the origin, $x_o(0, 0, 0)$. By Slivnyak's Theorem [32], if a point is placed at the origin the distribution of the point process is unchanged.

3) WBJs DEPLOYMENT

In this paper, we are concerned with the low-power jamming interference of the jammers. Since the WBJ's transmission power is very low, therefore, we considered WBJs to employ jamming interference. The WBJs are present in clusters and can be modeled as an MCP [6], [29]. The MCP constitutes of the parent-nodes, or clusters, and the child-nodes. In an MCP, the parent-nodes are excluded from the point process [33]. The parent-nodes are analogous to the number of clusters in the region of interest while the child-nodes are analogous to the number of WBJs in a cluster. In an MCP, the jamming clusters are distributed according to an independent HPPPs such that the density of the jamming cluster is set to λ_j, whereas, the jammers are distributed uniformly in a cluster of radius, r_j such that the average number of jammers in a cluster is set to $\bar{c}$. The density of the WBJs, λ_J, is therefore $\lambda_J = \lambda_j \bar{c}$.

B. JAMMING SCENARIO

The intentional radio-transmissions by the jammer aim to disrupt legitimate communication. This is typically

done by jamming contention- and channel-based access schemes [34]. In the jamming of contention-based access (such as carrier-sense multiple access (CSMA), CSMA with collision avoidance, etc.), a T-UE senses falsely that the medium is idle for signal transmission. Whereas, in the jamming of channel-based access (such as time division multiple access, frequency division multiple access, etc.), a T-UE's transmission is corruptly received at the receiver. This is done by transmitting at multiple channels of the shared medium. The jamming scenario mainly depends upon the transmission power of the radio, its location, and its effect on a T-UE [35]. In the aerial HetNets, signal-jamming occurs due to the presence of clustered-jammers in the proximity of a T-UE. Typically, the jamming scenario of the clustered-jammers considers proactive-, reactive-, and flow-jamming techniques for jamming legitimate UL communication [34]–[36].

In the proactive-jamming, the clustered-jammers jam UL legitimate communication by transmitting jamming interfering) signals in the transmission medium without considering that there is data transfer between the network-nodes [34], [35]. In contrast to the proactive-jamming, the clustered-jammers in the reactive-jamming, jam only when there is a network activity at a particular channel [35], [37]. Both these techniques operate on a single channel and are unable to switch to other channels for jamming purposes. Furthermore, these techniques are less energy-efficient due to their operation on a single channel. Whereas, in the flow-jamming technique, various jammers in a cluster coordinate with each other on multiple channels, either in a centralized or in a de-centralized manner to degrade the legitimate traffic-flow [35], [36]. In the centralized approach, multiple jammers compute the required transmission power and then transmit with the minimum radio-transmit power to jam the UL legitimate communication. While in the de-centralized approach, each jammer shares its information with the adjacent node to optimize the network's efficiency in terms of jamming.

C. CHANNEL FADING

In the aerial HetNets, when a LoS path is available between a T-UE and the serving UAV, our analysis follows Rician fading, and when there is no LoS (NLoS) path between a T-UE and the serving UAV, it follows Rayleigh fading. This type of channel fading is unified in Nakagami-m channel model, where m is the shape parameter of the Nakagami distribution and its value is characterized by the amplitudes of strong or weak components of the received signal. For the LoS link, $\mathrm{m} > 1$, and for the NLoS link, $\mathrm{m} = 1$. The probability density function of a random variable, X at a point, x in Nakagami-m model is (see, [38] for details)

$$f_X(x) = \frac{\mathrm{m}^{\mathrm{m}} x^{\mathrm{m}-1}}{\Omega^{\mathrm{m}} \Gamma(\mathrm{m})} \exp\left(-\frac{\mathrm{m}x}{\Omega}\right),$$

where Ω is the mean square value and $\Gamma(.)$ is the Gamma function [39].

D. SINGLE AND DUAL CONNECTIVITY

In aerial HetNets, SC allows a T-UE to maintain a single DL and UL connection by associating to either one or two UAVs. Whereas, dual connectivity feature allows a T-UE to maintain two connections in both DL and UL with more than one UAV simultaneously to exploit bandwidth and coverage resources [13], [15], [16].

1) SC WITH AND WITHOUT DECOUPLED ACCESS

In SC with DUDe access or decoupled access, a T-UE establishes its DL-connection on the basis of DL-reference received power (DRP) from the UAV while the UL-connection is established on the basis of maximum received signal strength at the UAV. Whereas, in SC with Non-DUDe or without decoupled access, a T-UE establishes its DL- and UL-connection on the basis of DRP from the UAV.

2) DC WITH DECOUPLED ACCESS

In DC strategy for two-tier aerial HetNets, a T-UE is allowed to maintain more than one connection with the UAVs simultaneously as shown in Fig. 2. In DC with DUDe or decoupled access for two-tier aerial HetNets, the first DL connection of a T-UE is established with the UAV of tier 1 on the basis of DRP (i.e., maximum signal strength at a T-UE from the UAV) while, the first UL connection is established on the basis of maximum received signal strength at the UAV of tier 2. Whereas, the second connection is the inverted-decoupled event such that the second UL is established with the UAV of tier 1 and second DL is established with the UAV of tier 2 [15], [17], [18]. This is practically valid for a network with fewer UAVs, so that the UE needs to establish second connection with the other tier's UAV by excluding the one already selected.

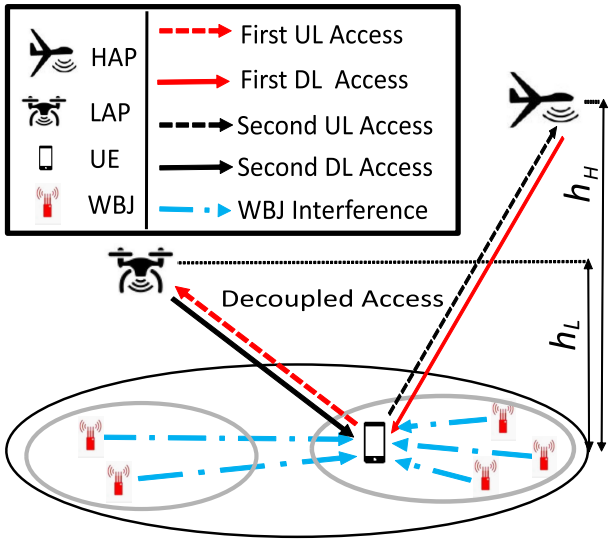

FIGURE 2. Dual connectivity and DL and UL decoupling for aerial HetNets in the presence to WBJs.

E. REVERSE FREQUENCY ALLOCATION

RFA is an efficient bandwidth allocation scheme where the DL frequency of the LAP-associated T-UE is allocated as the UL frequency for the HAP and the UL frequency of the HAP-associated T-UE is allocated as the DL frequency for the LAP [23], [40], [41].

For the 2-tier aerial HetNet considered in this work, an example deployment of the DC feature with RFA using 8 different frequencies is shown in Fig. 3 with these frequencies segregated by different colors. These frequencies are grouped into four categories on the basis of their association with the UAVs and on the basis of their association with the regions located inside or outside the coverage area of the UAVs. The regions located inside or outside the coverage area of the UAVs have significant importance for RFA. This is because the interference arising from these regions behaves differently at the serving UAVs. Since we are interested in the edge UEs located in the decoupled-enabled regions that can be specified by the regions, $A_H^{\mathbf{O}}$ and $A_L^{\mathbf{C}}$. Therefore, we mainly focus on the frequencies of these regions.

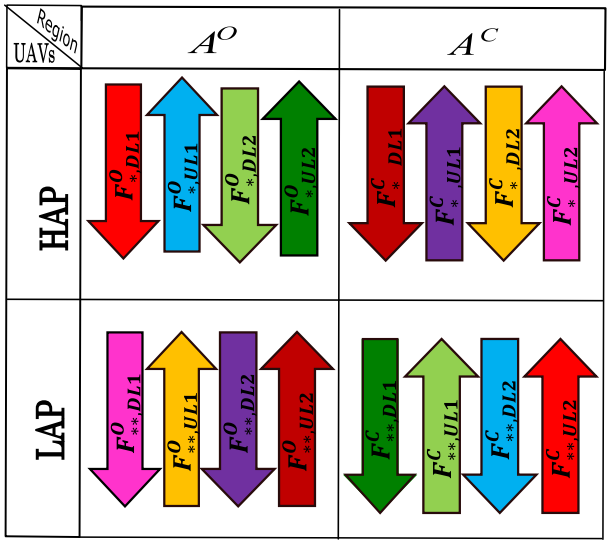

FIGURE 3. Bandwidth Allocation in a two-tier aerial HetNet with eight different frequencies. Each color denotes a unique frequency.

For the DC feature in aerial HetNets, the frequencies associated with the first DL connection of the HAPs and the LAPs are expressed as $F_{*,DL1}$, and $F_{**,DL1}$, respectively, and the first UL connection of the HAPs and the LAPs are expressed as $F_{*,UL1}$, and $F_{**,UL1}$, respectively. Furthermore, the frequencies associated with the first DL connection of the HAP and the LAP and with the regions located inside the coverage area of the UAVs (i.e., $A_H^{\mathbf{C}}$ and $A_L^{\mathbf{C}}$) are expressed as $F^{\mathbf{C}}_{*,DL1}$, and $F^{\mathbf{C}}_{**,DL1}$, respectively. While the frequencies associated with the first DL connection of the HAP and the LAP and with the regions located outside the coverage area of the UAVs (i.e., $A_H^{\mathbf{O}}$ and $A_L^{\mathbf{O}}$) are expressed as $F^{\mathbf{O}}_{*,DL1}$, and $F^{\mathbf{O}}_{**,DL1}$, respectively. Similarly, the frequencies associated with the first UL connection of the HAP and the LAP and with the regions located inside the coverage area of the UAVs are expressed as $F^{\mathbf{C}}_{*,UL1}$, and $F^{\mathbf{C}}_{**,UL1}$, respectively. While the frequencies associated with the first UL connection of the HAP and the LAP and with the regions located outside the coverage area of the UAVs are expressed as $F^{\mathbf{O}}_{*,UL1}$, and $F^{\mathbf{O}}_{**,UL1}$. Similarly, the frequencies are allocated to the HAPs and LAPs of the second DL and second UL connections.

F. RECEIVED-POWER AND SIGNAL-TO-INTERFERENCE-RATIO

1) RECEIVED-POWER

The average received-power at a T-UE from the i-th tier UAV is $\mathbb{E}[\mathcal{S}] = P_i \parallel X_i \parallel^{-\alpha_i}$, where P_i is the transmit power of i-th tier UAV such that $i\epsilon\{H, L\}$, $||X_i||$ is Euclidean-distance between a T-UE located at the origin and i-th tier UAV, and α_i is the pathloss exponent of tier i with the assumption that $\alpha_i > 2$ (see [6], [11] for details). The average received-power at the i-th tier UAV from a T-UE is $\mathbb{E}[\mathcal{S}] = Q_i \parallel X_i \parallel^{-\alpha_i}$, where Q_i is the UE's transmission power associated to a UAV of tier i.

2) SIGNAL-TO-INTERFERENCE-RATIO

The UL signal-to-interference-ratio (SIR) is defined as the ratio of received-power by a typical UAV to the received-interference at that UAV. The SIR of the first UL connection in DC with the decoupled access is expressed as

$$\mathrm{SIR}_L^{UL} \triangleq \frac{Q_L g_L \parallel X_L \parallel^{-\alpha_L}}{\mathcal{I}^{UL}_{\Phi_{L,A_H^{\mathbf{O}}}} + \mathcal{I}^{DL}_{\Phi_{H,A_L^{\mathbf{C}}}} + \mathcal{I}_{\Phi_{J,L}}}, \tag{1}$$

where g_L is the amplitude of the Nakagami-m distributed fading channel between the LAP and a T-UE such that channel power gain is Gamma distributed with shape parameter, m and scale parameter, 1/m, $\mathcal{I}^{UL}_{\Phi_{L,A_H^{\mathbf{O}}}}$ is the UL interference at the LAP from the UEs that are located outside the coverage area of the HAP, $\mathcal{I}^{DL}_{\Phi_{H,A_L^{\mathbf{C}}}}$ is the DL interference at the LAP from the HAPs that are located inside the coverage area of the LAP, and $\mathcal{I}_{\Phi_{J,L}}$ is the interference of the WBJs at the LAP. Furthermore, the UL interference from the UEs located outside the coverage area of the HAP is defined as $\mathcal{I}^{UL}_{\Phi_{L,A_H^{\mathbf{O}}}} = \sum_{k\epsilon\Phi_{I_{L,A_H^{\mathbf{O}}}}} Q_L g_k \parallel X_k - X_L \parallel^{-\alpha_L}$, where k represents the k-th interferer of the interfering process, $\Phi_{I_{L,A_H^{\mathbf{O}}}}$. Nevertheless, the DL interference of the HAPs located inside the coverage area of the LAP is defined as $\mathcal{I}^{DL}_{\Phi_{H,A_L^{\mathbf{C}}}} = \sum_{v\epsilon\Phi_{I_{H,A_L^{\mathbf{C}}}}} P_H g_v \parallel X_v - X_H \parallel^{-\alpha_H}$, where v represents the v-th interferer of the interfering process, $\Phi_{I_{H,A_L^{\mathbf{C}}}}$. Additionally, the interference of the WBJs at the LAP is defined as $\mathcal{I}_{\Phi_{J,L}} = \sum_{l\epsilon\Phi_J} P_j g_l \parallel X_l - X_L \parallel^{-\alpha_L}$, where l represents the l-th jammer of the jammers' process, $\Phi_{J,L}$ and P_j represents the transmit power of the jammer.

Similarly, the SIR of the second UL connection is

$$\mathrm{SIR}_H^{UL} \triangleq \frac{Q_H g_H \parallel X_H \parallel^{-\alpha_H}}{\mathcal{I}^{UL}_{\Phi_{H,A_H^{\mathbf{O}}}} + \mathcal{I}^{DL}_{\Phi_{L,A_L^{\mathbf{C}}}} + \mathcal{I}_{\Phi_{J,H}}}, \tag{2}$$

where g_H is the amplitude of the Nakagami-m distributed fading channel between the HAP and a T-UE such that channel power gain is Gamma distributed with shape parameter, m and scale parameter, 1/m, $\mathcal{I}^{UL}_{\Phi_{H,A_H^{\mathbf{O}}}}$ is the UL interference at the HAP from the UEs that are located outside the coverage area of the HAP, $\mathcal{I}^{DL}_{\Phi_{L,A_L^{\mathbf{C}}}}$ is the DL interference at the HAP from the LAPs that are located inside the coverage area of the LAP, and $\mathcal{I}_{\Phi_{J,H}}$ is the interference of the WBJs at the HAP. Moreover, the UL interference from the UEs that are located outside the coverage area of the HAP is defined as $\mathcal{I}^{UL}_{\Phi_{H,A_H^{\mathbf{O}}}} = \sum_{\bar{k}\epsilon\Phi_{I_{H,A_H^{\mathbf{O}}}}} Q_H g_{\bar{k}} \parallel X_{\bar{k}} - X_H \parallel^{-\alpha_H}$, where $\bar{k}$ represents the $\bar{k}$-th interferer of the interfering process, $\Phi_{I_{H,A_H^{\mathbf{O}}}}$. Furthermore, the DL interference of the LAPs that are located inside the coverage area of the LAP is defined as $\mathcal{I}^{DL}_{\Phi_{L,A_L^{\mathbf{C}}}} = \sum_{\bar{v}\epsilon\Phi_{I_{L,A_L^{\mathbf{C}}}}} P_L g_{\bar{v}} \parallel X_{\bar{v}} - X_L \parallel^{-\alpha_L}$, where $\bar{v}$ represents the $\bar{v}$-th interferer of the interfering process, $\Phi_{I_{L,A_L^{\mathbf{C}}}}$. Further, the interference of the WBJs at the HAP is defined as $\mathcal{I}_{\Phi_{J,H}} = \sum_{\bar{l}\epsilon\Phi_J} P_j g_{\bar{l}} \parallel X_{\bar{l}} - X_H \parallel^{-\alpha_H}$, where $\bar{l}$ represents the $\bar{l}$-th jammer of the jammers' process, $\Phi_{J,H}$.

We also consider τ as the received SIR threshold value. Similar to [42], we assumed orthogonal frequency division multiple access such that the UEs associated with the same UAV does not interfere in UL. Furthermore, the density of UEs is given by $\lambda_U \gg \lambda_H + \lambda_L$.

III. PRELIMINARIES

Here, we first derive the association probability of the serving UAV. Then, we derive probability density function (PDF) between the serving UAV and a T-UE and then, the UL and DL interference at the serving UAV. We further derive the received interference due to WBJs.

A. ASSOCIATION PROBABILITY OF THE DECOUPLING-ENABLED REGION

Here, we focus on the decoupled access for the edge users or the UEs that are present in the decoupled-enabled regions because decoupling UL and DL for the decoupled-enabled regions provides higher gains [6], [43], [44]. The decoupled-enabled region is a 2-dimensional region, where a higher power from the HAP is obtained at the T-UE whereas, a higher power from the same T-UE is obtained at the LAP.

The physical meaning of the associated probability of the T-UEs located in the decoupled-enabled region depicts the probability of the T-UEs that can associate with the LAP in UL, while with the HAP in DL. Since the UEs located in the decoupled-enabled regions provide sub-optimal performance by adopting the SC access [15], [17], [18]. Therefore, in this paper, we focus on the access scheme that optimizes the performance of the UEs located in the decoupled-enabled regions by adopting the DC strategy. The association probability of a T-UE that is present in the decoupled-enabled region is derived in the Appendix A and is expressed as [6]:

$$\begin{aligned}\mathbb{A}_D &= \frac{\alpha_H}{2\alpha_L}\left(\mathcal{H}^{1,1}_{1,1}\left[\frac{(\sqrt{\pi\lambda_H})\frac{\alpha_H}{\alpha_L}\left(\frac{Q_H}{Q_L}\right)^{\frac{1}{\alpha_L}}}{\sqrt{\pi\lambda_L}}\middle|\begin{matrix}\left(0,\frac{1}{2}\right)\\ \left(0,\frac{\alpha_H}{2\alpha_L}\right)\end{matrix}\right]\right.\\ &\left. - \mathcal{H}^{1,1}_{1,1}\left[\frac{(\sqrt{\pi\lambda_H})^{\alpha_H/\alpha_L}\left(\frac{P_H}{P_L}\right)^{1/\alpha_L}}{\sqrt{\pi\lambda_L}}\middle|\begin{matrix}\left(0,\frac{1}{2}\right)\\ \left(0,\frac{\alpha_H}{2\alpha_L}\right)\end{matrix}\right]\right),\end{aligned} \tag{3}$$

where $\mathcal{H}^{1,1}_{1,1}\left[-\middle|\begin{matrix}(-,-)\\(-,-)\end{matrix}\right]$ is a Fox H-function with parameter values set to $m_1 = 1, n_1 = 1, v_1 = 1, w_1 = 1$ in (19) (see Appendix A and [45]).

B. PDF OF DISTANCE TO THE SERVING UAV

Similar to [6], [20], [46], we investigate the performance of the aerial HetNets in terms of the coverage probability by deriving the PDF of the distance-distribution between the UAV and a T-UE that is located at the cell-edge or the decoupled-enabled region.

For the decoupled-enabled region, the PDF of the distance of the first UL connection means that there isn't any LAP closer than x in the decoupled-enabled region that can create interference at the serving station. Thus, all the interferers are located at a distance larger than x. For the first UL connection in the decoupled-enabled region, the PDF of the distance between the serving LAP and a T-UE that is present in the decoupled-enabled region is derived in Appendix B and is expressed as [6]:

$$\begin{aligned}f^{(UL1)}_{X_L}(x) = &\left(\exp\left\{-\pi\lambda_H\left(\frac{P_H}{P_L}\right)^{\frac{2}{\alpha_H}} x^{\frac{2\alpha_L}{\alpha_H}}\right\}\right.\\ &\left. - \exp\left\{-\pi\lambda_H\left(\frac{Q_H}{Q_L}\right)^{\frac{2}{\alpha_H}} x^{\frac{2\alpha_L}{\alpha_H}}\right\}\right)\frac{f_{X_L}(x)}{\mathbb{A}_D}.\end{aligned} \tag{4}$$

For the decoupled-enabled region, the physical meaning of the PDF of the distance of the second UL connection means that no HAP is closer than x in the region-of-interest that can introduce interference at the serving UAV. Thus, no interferer is located within a distance of x. We follow similar steps of Appendix B to derive the PDF of the distance of the second UL connection between the serving HAP and a T-UE in the decoupled-enabled region. For the second UL connection in the decoupled-enabled region, the PDF of the distance of

the second UL connection between the HAP and a T-UE is:

$$f_{X_H}^{(UL2)}(x)=\left(\exp\left\{-\pi\lambda_L\left(\frac{P_L}{P_H}\right)^{\frac{2}{\alpha_L}}{}_x\frac{2\alpha_H}{\alpha_L}\right\}-\exp\left\{-\pi\lambda_L\left(\frac{Q_L}{Q_H}\right)^{\frac{2}{\alpha_L}}{}_x\frac{2\alpha_H}{\alpha_L}\right\}\right)\frac{f_{X_H}(x)}{\mathbb{A}_D}. \quad (5)$$

C. INTERFERENCE AT THE SERVING UAV

Here, we characterize UL and DL interference at the serving UAV and the interference of the WBJs at the serving UAV.

1) UL AND DL INTERFERENCE AT THE SERVING UAV

In this paper, we employ DC and RFA for the decoupled aerial HetNets. The serving UAV in the decoupled access is the LAP while the serving UAV in the non-decoupled access is the HAP. Therefore, the characterization of the interference at the serving UAVs is indispensable.

For the first UL connection with the decoupled access in the decoupled-enabled region, the interference from outside the coverage area of the HAP is expressed in [7] and also driven in Appendix C is

$$\mathcal{L}_{\mathcal{I}^{UL}_{\Phi_{L,A^{\mathbf{O}}_H}}}(s)=\exp\left\{\frac{2\pi\lambda_L\tau r_2^{2-\alpha_L}}{x^{-\alpha_L}(\alpha_L-2)}{}_2F_1(1,1-\frac{2}{\alpha_L};2-\frac{2}{\alpha_L};-\tau\left(\frac{x}{r_2}\right)^{\alpha_L})-\frac{2\pi\lambda_L\tau r_1^{2-\alpha_L}}{x^{-\alpha_L}(\alpha_L-2)}{}_2F_1(1,1-\frac{2}{\alpha_L};2-\frac{2}{\alpha_L};-\tau\left(\frac{x}{r_1}\right)^{\alpha_L})\right\}, \quad (6)$$

where ${}_2F_1(-,-;-;-)$ is the Hyper-geometric function [39]. Similarly, following Appendix C, the UL interference at the serving HAP from outside the circular-radius of the HAP is expressed as

$$\mathcal{L}_{\mathcal{I}^{UL}_{\Phi_{H,A^{\mathbf{O}}_H}}}(s)=\exp\left\{\frac{2\pi\lambda_H\tau r_2^{2-\alpha_H}}{x^{-\alpha_H}(\alpha_H-2)}{}_2F_1(1,1-\frac{2}{\alpha_H};2-\frac{2}{\alpha_H};-\tau\left(\frac{x}{r_2}\right)^{\alpha_H})-\frac{2\pi\lambda_H\tau r_1^{2-\alpha_H}}{x^{-\alpha_H}(\alpha_H-2)}{}_2F_1(1,1-\frac{2}{\alpha_H};2-\frac{2}{\alpha_H};-\tau\left(\frac{x}{r_1}\right)^{\alpha_H})\right\}. \quad (7)$$

Following the steps in Appendix C and assuming that the ratio of the transmission power of the HAP to the UE connected with the LAP as ζ_L^H; Laplace transform at the serving HAP from the UEs located in the circular-radius of the LAP is obtained as:

$$\mathcal{L}_{\mathcal{I}^{DL}_{\Phi_{H,A^{\mathbf{C}}_L}}}(s)=\exp\left\{\frac{2\pi\zeta_L^H\lambda_H\tau z_1^{2-\alpha_H}}{x^{-\alpha_H}(\alpha_H-2)}{}_2F_1(1,1-\frac{2}{\alpha_H};2-\frac{2}{\alpha_H};-\zeta_L^H\tau\left(\frac{x}{z_1}\right)^{\alpha_H})-\frac{2\pi\zeta_L^H\lambda_H\tau z_0^{2-\alpha_H}}{x^{-\alpha_H}(\alpha_H-2)}{}_2F_1(1,1-\frac{2}{\alpha_H};2-\frac{2}{\alpha_H};-\zeta_L^H\tau\left(\frac{x}{z_0}\right)^{\alpha_H})\right\}. \quad (8)$$

Similarly, following the steps in Appendix C and assuming that the ratio of the transmission power of the LAP to the UE connected with the HAP as ζ_H^L; Laplace transform at the serving LAP from the circular-radius of the LAP is

$$\mathcal{L}_{\mathcal{I}^{DL}_{\Phi_{L,A^{\mathbf{C}}_L}}}(s)=\exp\left\{\frac{2\pi\zeta_H^L\lambda_L\tau z_1^{2-\alpha_L}}{x^{-\alpha_L}(\alpha_L-2)}{}_2F_1(1,1-\frac{2}{\alpha_L};2-\frac{2}{\alpha_L};-\zeta_H^L\tau\left(\frac{x}{z_1}\right)^{\alpha_L}-\frac{2\pi\zeta_H^L\lambda_L\tau z_0^{2-\alpha_L}}{x^{-\alpha_L}(\alpha_L-2)}{}_2F_1(1,1-\frac{2}{\alpha_L};2-\frac{2}{\alpha_L};-\zeta_H^L\tau\left(\frac{x}{z_0}\right)^{\alpha_L})\right\}. \quad (9)$$

2) INTERFERENCE OF THE WBJs

The MCP-distributed WBJs exploit the legitimate UL transmission between a T-UE and the serving UAV using WBJ's interference. Laplace transform of WBJ's interference at the i-th tier UAV is expressed as [7] and driven in Appendix D is

$$\mathcal{L}_{\mathcal{I}_{\Phi_{J,i}}}(s)=\exp\left\{-\frac{2\pi\bar{c}\Delta_i x^2\tau^{2/\alpha_i}}{\alpha_i r_j^2}\csc\left(\frac{2\pi}{\alpha_i}\right)-\lambda_j\pi\Delta_i\tau^{2/\alpha_i}x^2\int_0^\infty\left(1-\exp\left\{\frac{-\bar{c}}{1+t^{\alpha_i/2}}\right\}\right)dt\right\}. \quad (10)$$

IV. ANALYSIS OF UPLINK COVERAGE PROBABILITY

The probability that the received UL SIR at the serving UAV of tier i is larger than the pre-defined value is defined as the UL coverage probability and is given as [6]

$$\mathcal{C}^{UL}\triangleq\mathbb{E}_{X_i}\left\{\mathbb{P}\{\mathrm{SIR}^{UL}_{X_i}>\tau\}\right\}. \quad (11)$$

The coverage probability of the first UL-connection in DC with the decoupled access is referred to as the probability that the UL SIR at the serving LAP is larger than the pre-defined SIR-threshold and is expressed as

$$\mathcal{C}^{UL1}\triangleq\mathbb{E}_{X_L}\left\{\mathbb{P}\{\mathrm{SIR}^{UL}_{X_L}>\tau\}\right\}. \quad (12)$$

The coverage probability of the first UL connection in DC with the decoupled access is driven as

$$\mathcal{C}^{UL1}\triangleq\int_{r_1}^{r_2}\mathbb{P}\{\mathrm{SIR}^{UL}_{X_L}>\tau\}f_{X_L}^{(UL1)}(x)dx\overset{a}{=}\int_{r_1}^{r_2}\mathbb{P}\left\{\frac{Q_L g_L\parallel X_L\parallel^{-\alpha_L}}{\mathcal{I}^{UL}_{\Phi_{L,A^{\mathbf{O}}_H}}+\mathcal{I}^{DL}_{\Phi_{H,A^{\mathbf{C}}_L}}+\mathcal{I}_{\Phi_{J,L}}}>\tau\right\}f_{X_L}^{(UL1)}(x)dx$$

$$\stackrel{b}{=} \int_{r_1}^{r_2} \mathbb{E}\left\{ g_L > \frac{\tau x^{\alpha_L}}{Q_L}\left(\mathcal{I}^{UL}_{\Phi_{L,A^{\mathbf{O}}_H}} + \mathcal{I}^{DL}_{\Phi_{H,A^{\mathbf{C}}_L}} + \mathcal{I}_{\Phi_{J,L}}\right)\right\} \times f^{(UL1)}_{X_L}(x)dx$$
$$\stackrel{c}{=} \int_{r_1}^{r_2} \mathbb{E}\left\{\exp\left(-s\mathcal{I}^{UL}_{\Phi_{L,A^{\mathbf{O}}_H}}\right)\right\}\mathbb{E}\left\{\exp\left(-s\mathcal{I}^{DL}_{\Phi_{H,A^{\mathbf{C}}_L}}\right)\right\} \times \mathbb{E}\left\{\exp\left(-s\mathcal{I}_{\Phi_{J,L}}\right)\right\} f^{(UL1)}_{X_L}(x)dx$$
$$\stackrel{d}{=} \int_{r_1}^{r_2} \mathcal{L}_{\mathcal{I}^{UL}_{\Phi_{L,A^{\mathbf{O}}_H}}}(s)\mathcal{L}_{\mathcal{I}^{DL}_{\Phi_{H,A^{\mathbf{C}}_L}}}(s)\mathcal{L}_{\mathcal{I}_{\Phi_{J,L}}}(s) f^{(UL1)}_{X_L}(x)dx, \quad (13)$$

where $\stackrel{a}{=}$ is obtained by substituting (1) in (12), $\stackrel{b}{=}$ is obtained by simple mathematics, $\stackrel{c}{=}$ is obtained by assuming the parameters of fading channel as $\mathrm{m} = 1$ and $\Omega = 1$ for the NLoS communication, and $\stackrel{d}{=}$ is obtained by using Laplace transform. The final expression is obtained by substituting (6), (8), and (10) in (13) and is expressed in (14), as shown at the bottom of the page.

The coverage probability of the second UL connection is defined as the probability that the UL SIR at the serving HAP is larger than the pre-defined SIR-threshold,

$$\mathcal{C}^{UL2} \triangleq \mathbb{E}_{X_H}\left\{\mathbb{P}\{\mathrm{SIR}^{UL}_{X_H} > \tau\}\right\}. \quad (15)$$

The coverage probability of the second connection along with RFA and WBJs is derived as

$$\mathcal{C}^{UL2} \triangleq \int_{r_1}^{r_2} \mathbb{P}\{\mathrm{SIR}^{UL}_{X_H} > \tau\} f^{(UL2)}_{X_H}(x)dx$$
$$\stackrel{a}{=} \int_{r_1}^{r_2} \mathbb{P}\left\{\frac{Q_H g_H \parallel X_H \parallel^{-\alpha_H}}{\mathcal{I}^{UL}_{\Phi_{H,A^{\mathbf{O}}_H}} + \mathcal{I}^{DL}_{\Phi_{L,A^{\mathbf{C}}_L}} + \mathcal{I}_{\Phi_{J,H}}} > \tau\right\} f^{(UL2)}_{X_H}(x)dx$$
$$\stackrel{b}{=} \int_{r_1}^{r_2} \mathbb{E}\left\{g_H > \frac{\tau x^{\alpha_H}}{Q_H}\left(\mathcal{I}^{UL}_{\Phi_{H,A^{\mathbf{O}}_H}} + \mathcal{I}^{DL}_{\Phi_{L,A^{\mathbf{C}}_L}} + \mathcal{I}_{\Phi_{J,H}}\right)\right\} \times f^{(UL2)}_{X_H}(x)dx$$
$$\stackrel{c}{=} \int_{r_1}^{r_2} \mathbb{E}\left\{\exp\left(-s\mathcal{I}^{UL}_{\Phi_{H,A^{\mathbf{O}}_H}}\right)\right\}\mathbb{E}\left\{\exp\left(-s\mathcal{I}^{DL}_{\Phi_{L,A^{\mathbf{C}}_L}}\right)\right\} \times \mathbb{E}\left\{\exp\left(-s\mathcal{I}_{\Phi_{J,H}}\right)\right\} f^{(UL2)}_{X_H}(x)dx$$
$$\stackrel{d}{=} \int_{r_1}^{r_2} \mathcal{L}_{\mathcal{I}^{UL}_{\Phi_{H,A^{\mathbf{O}}_H}}}(s)\mathcal{L}_{\mathcal{I}^{DL}_{\Phi_{L,A^{\mathbf{C}}_L}}}(s)\mathcal{L}_{\mathcal{I}_{\Phi_{J,H}}}(s) f^{(UL2)}_{X_H}(x)dx, \quad (16)$$

where $\stackrel{a}{=}$ is obtained by substituting (2) in (15), $\stackrel{b}{=}$ is obtained by simple mathematical-manipulations, $\stackrel{c}{=}$ is obtained by assuming fading channel parameters as $\mathrm{m} = 1$ and $\Omega = 1$ for the NLoS communication, and $\stackrel{d}{=}$ is obtained by Laplace transform. The final expression of the coverage probability of the second UL-connection along with the RFA and WBJs is obtained by substituting (7), (9), and (10) in (16) and is expressed in (17), as shown at the bottom of the next page. Finally, the coverage probability of the DC feature in UL follows by considering that at least one of the link is in coverage, i.e., $1 - (1 - \mathcal{C}^{UL1})(1 - \mathcal{C}^{UL2})$.

Similarly, the UL coverage probability of the SC with DUDe access and SC with Non-DUDe access can be derived following the derivation of (14) and (17), respectively. Note that the bandwidth utilized by SC with DUDe or the decoupled access and SC with Non-DUDe or the non-decoupled access is twice the bandwidth of DC with DUDe or the decoupled access.

V. RESULTS AND DISCUSSION

In this section, we describe the results of the coverage probability of the first and second UL connection of a T-UE in comparison with the results of the UL coverage probability of a T-UE in the SC mode. The simulation setup assumes that each T-UE has DC functionality and is equipped with multiple-radio transmitters and receivers. This is because each T-UE is allowed to transmit and receive on two separate UL and DL connections simultaneously. Furthermore, to ensure reliable data-delivery in aerial HetNets, each T-UE operates on a set of eight different frequencies instead of four frequencies (such as in SC mode). For a two-tier aerial HetNet with DC functionality, a T-UE establishes its first UL connection with the tier of the UAV that receives its maximum signal power, and the second UL connection is established with the tier of the UAV (excluding the already-connected tier) that receives its second maximum signal power. Whereas, for the SC mode, a T-UE establishes its UL connection either on the basis of maximum DRP (such as in SC with DRP access) or on the basis of the maximum power received at the UAV (such as in SC with DUDe access).

$$\mathcal{C}^{UL1} = \int_{r_1}^{r_2} \exp\left(\pi\tau x^{\alpha_L}\left[\frac{\lambda_L}{\alpha_L/2-1} r_2^{2-\alpha_L} {}_2F_1(1, 1-\frac{2}{\alpha_L}; 2-\frac{2}{\alpha_L}; -\tau\left(\frac{x}{r_2}\right)^{\alpha_L}) - \frac{\lambda_L}{\alpha_L/2-1} r_1^{2-\alpha_L} {}_2F_1(1, 1-\frac{2}{\alpha_L}; 2-\frac{2}{\alpha_L}; -\tau\left(\frac{x}{r_1}\right)^{\alpha_L}) + \frac{\lambda_H}{\alpha_H/2-1}\zeta_L^H z_1^{2-\alpha_H} {}_2F_1(1, 1-\frac{2}{\alpha_H}; 2-\frac{2}{\alpha_H}; -\zeta_L^H\tau\left(\frac{x}{z_1}\right)^{\alpha_H}) - \frac{\lambda_H}{\alpha_H/2-1}\zeta_L^H z_0^{2-\alpha_H} {}_2F_1(1, 1-\frac{2}{\alpha_H}; 2-\frac{2}{\alpha_H}; -\zeta_L^H\tau\left(\frac{x}{z_0}\right)^{\alpha_H})\right] - x^2\Delta_L\tau^{2/\alpha_L}\frac{2\pi\bar{c}}{\alpha_L r_j^2}\csc\left(\frac{2\pi}{\alpha_L}\right) - \lambda_j\pi\tau^{2/\alpha_L}\Delta_L x^2\int_0^\infty\left(1 - \exp\left\{\frac{-\bar{c}}{1+t^{\alpha_L/2}}\right\}\right)dt\right) f^{(UL1)}_{X_L}(x)xdx. \quad (14)$$

The analytical results are validated using 100,000 independent Monte-Carlo trials. Unless otherwise stated, the following simulation parameters are set to enable a fair comparison with the work in [7]: the density of the HAP and the LAP is set as $1/\pi 1000^2 \text{m}^2$ and $2/\pi 1000^2 \text{m}^2$, respectively. The transmission power of the HAP, LAP, and jammer is set as 46 dBm, 30 dBm, and 10 dBm, respectively while, the pathloss exponent of the HAP and the LAP is set as 2.75 and 3, respectively. The transmission power of the HAP- and LAP-associated T-UE is set as 30 dBm while the height of the HAP and the LAP is set as 300 m and 100 m, respectively. The density of the clustered-jammers is set as $1/\pi 1000^2$ m^2. The radius of the jamming cluster is 100 m and the SIR threshold for the successful coverage event is set to -20 dB. The bandwidth of the first and the second link in DC with DUDe is set as 10 MHz thus the total bandwidth, B is equal to 20 MHz. Furthermore, the total bandwidth of the SC with DUDe access and the SC with Non-DUDe access is 20 MHz for a fair comparison with the DC system.

Fig. 4 shows the coverage probability of a T-UE in UL against the SIR threshold. The coverage probability of a T-UE using DC with DUDe access is significantly higher than that of the SC with DUDe access and the SC with Non-DUDe access. This is because the UL coverage probability of the DC with DUDe access is obtained by assuming that at least one of the links is in coverage, i.e., $1-(1-\mathcal{C}^{UL1})(1-\mathcal{C}^{UL2})$. The UL coverage probability of a T-UE in aerial HetNets decreases with the number of jammers. This is because the jamming interference (which depends upon the number of WBJs) is increased with the number of jammers. The coverage probability of the DC with DUDe access decreases up to 10.6% with the increase in the number of jammers up to 4 per cluster at -20 dB. It is observed that for the SIR threshold of -20 dB and without jamming, the percentage-increase in terms of the coverage probability of the DC with DUDe over the SC with DUDe and Non-DUDe access is 10.6% and 82.6%, respectively.

Fig. 5 shows the UL coverage probability of a T-UE against the transmission power of the UE that is associated with the LAP. The UL coverage probability of the T-UE increases by increasing the transmission power of the UE that is associated with the LAP because with the increase in the transmission power of a T-UE, more UEs are added to the decoupled-enabled regions. As a result, the association probability is increased which results in increasing the

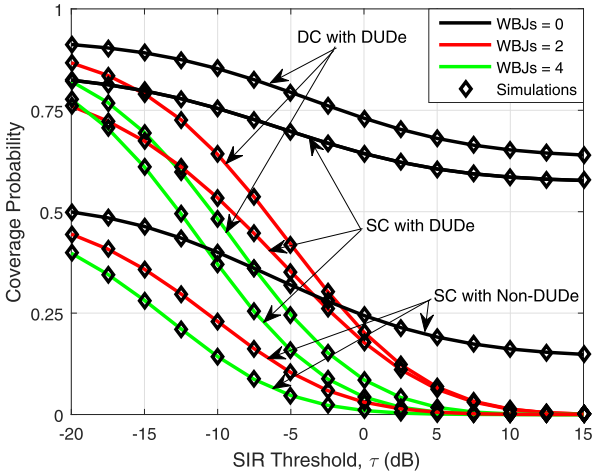

FIGURE 4. The effect of the different number of jammers and the SIR-threshold on the UL coverage probability.

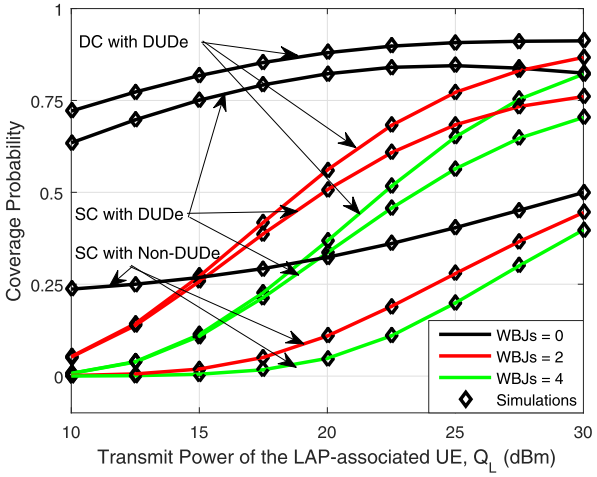

FIGURE 5. The effect of the different number of jammers and the transmission power of the UE associated to LAP on the UL coverage probability.

$$\begin{aligned}\mathcal{C}^{UL2} = \int_{r_1}^{r_2} \exp\Bigg(\pi\tau x^{\alpha_H}\Bigg[&\frac{2\lambda_H}{\alpha_H-2} r_2^{2-\alpha_H}\, {}_2F_1\Big(1,1-\frac{2}{\alpha_H};2-\frac{2}{\alpha_H};\\ &-\tau\left(\frac{x}{r_2}\right)^{\alpha_H}\Big) - \frac{2\lambda_H}{\alpha_H-2} r_1^{2-\alpha_H}\, {}_2F_1\Big(1,1-\frac{2}{\alpha_H};2-\frac{2}{\alpha_H};-\tau\left(\frac{x}{r_1}\right)^{\alpha_H}\Big)\\ &+\frac{2\lambda_L}{\alpha_L-12}\zeta_H^L z_1^{2-\alpha_L}\, {}_2F_1\Big(1,1-\frac{2}{\alpha_L};2-\frac{2}{\alpha_L};-\zeta_H^L\tau\left(\frac{x}{z_1}\right)^{\alpha_L}\Big)\\ &-\frac{2\lambda_L}{\alpha_L-2}\zeta_H^L z_0^{2-\alpha_L}\, {}_2F_1\Big(1,1-\frac{2}{\alpha_L};2-\frac{2}{\alpha_L};-\zeta_H^L\tau\left(\frac{x}{z_0}\right)^{\alpha_L}\Big)\Bigg]\\ &-x^2\Delta_H\tau^{2/\alpha_H}\frac{2\pi\bar{c}}{\alpha_H r_j^2}\csc\left(\frac{2\pi}{\alpha_H}\right)-\lambda_j\pi\tau^{2/\alpha_H}\Delta_H x^2\int_0^\infty\left(1-\exp\left\{\frac{-\bar{c}}{1+t^{\alpha_H/2}}\right\}\right)dt\Bigg) f_{X_H}^{(UL2)}(x)x dx. \end{aligned} \tag{17}$$

coverage performance. The coverage performance of the DC with DUDe access increases up to 26.4% with the increase in Q_L from 10 dBm to 30 dBm. The UL coverage probability of a T-UE in aerial HetNets is decreased with the increase of the number of jammers per cluster because the jamming interference (that depends upon the number of WBJs) is increased by increasing WBJs.

The UL coverage probability of the DC with DUDe access is significantly higher than that of the SC with DUDe and the SC with Non-DUDe access because it is obtained by assuming that at least one of the links is in coverage. Note that the gain in the coverage probability of the SC with DUDe over the SC with Non-DUDe is high as compared to the gain in the coverage probability of the DC with DUDe over the SC with DUDe. However, the probability that a link in a single connectivity mode is always serving and never disconnects is much lower. This is because of clustered-jammers and frequent handovers. This adversely affects the reliable delivery of data at the receiving node. To address this issue and to maintain reliable communication in aerial HetNets, a T-UE must maintain multiple connections with the UAV. Eventually, a trade-off is expected between communication reliability disrupting DC mode and its implementation cost in terms of complexity and energy efficiency.

Fig. 6 shows the UL coverage probability of a T-UE against the transmission power of the LAP. The UL coverage probability of the T-UE decreases with the transmission power of the LAP because the UEs are excluded from the decoupled-enabled region with the increase in the transmission power of the LAP. As a result, the association probability is decreased which results in decreasing the coverage probability. It is noteworthy that for the RFA strategy, the transmit power of the UAVs can create interference in the UL, therefore, UL coverage is degraded. Thus, the coverage probability of the DC with DUDe access and without WBJs decreases up to 7.4% with the increase in P_L from 20 dBm to 30 dBm.

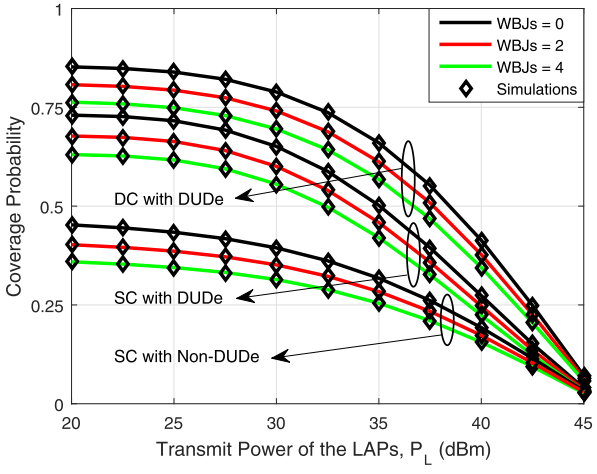

FIGURE 6. The effect of the different number of jammers and the transmit power of the LAP on the UL coverage probability.

Fig. 7 shows the UL coverage probability of a T-UE against the radius of the clustered-jammers. The UL coverage probability of the T-UE increases with the increase in the radius of the clustered-jammers. This is because when the radius of the cluster is increased; the jammers are allowed to be randomly located in a geographically larger region. Thus, the cumulative power of jamming signals is reduced at a T-UE. As a result, the coverage probability is improved. Moreover, the coverage probability of the DC with DUDe access is increased up to 17.9% with the increase in radius from 50 m to 100 m for the jammers set to 2.

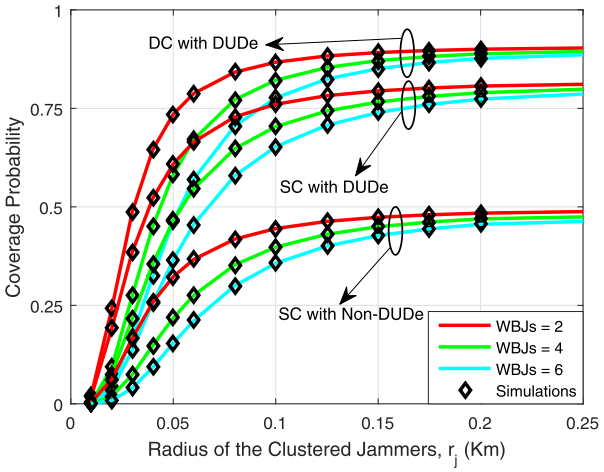

FIGURE 7. The effect of the different number of jammers and their cluster radius on the UL coverage probability.

Fig. 8 shows the UL coverage probability of a T-UE against the transmission power of the jammers. The UL coverage probability of the T-UE is decreased with the increase in the transmit power of the jammers because the power of jamming interference at the T-UE is increased. As a result, UL coverage probability is decreased. Moreover, the coverage probability of the DC with DUDe access decreases up to 13% with the increase in P_j from 5 dBm to 15 dBm for the jammers set to 2.

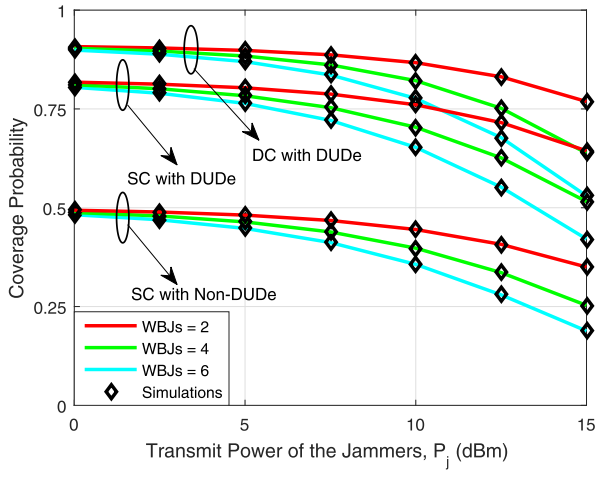

FIGURE 8. The effect of the different number of jammers and their transmit power on the UL coverage probability.

VI. CONCLUSION

This work analyzed the coverage performance of a two-tier aerial HetNet that employs dual-connectivity jointly with decoupled access and reverse frequency allocation in the presence of clustered-jammers. The serving UAVs and T-UEs were modeled using independent HPPPs while the WBJs, assumed to be spatially clustered, were modeled by the MCP. The performance of the aerial HetNets was analyzed in terms of the UL coverage probability and it was shown that the functionality of DC with DUDe access is better than that of the SC with DUDe access and SC with Non-DUDe access in the presence of RFA and WBJs. Moreover, aerial HetNets-performance is increased with the increase in the transmission power of a T-UE associated with LAP and the increase in the radius of the jammers cluster while it decreases with the increase of the transmission power of the LAP and the WBJs.

APPENDIX A
DERIVATION OF (3)

The connection between the UAV of tier i and a T-UE describes that within a sphere of radius, x there isn't any interfering UAV closer than the serving UAV. The probability density function (PDF) between the UAV of tier i and a T-UE is given as [32], [47]

$$f_{X_i}(x) = 2\pi\lambda_i e^{-\pi\lambda_i x^2}. \tag{18}$$

In the decoupled access, the association probability of a T-UE is derived as [6]:

$$\mathbb{A}_D = \mathbb{P}\left\{P_H X_H^{-\alpha_H} > P_L X_L^{-\alpha_L}; Q_H X_H^{-\alpha_H} \leq Q_L X_L^{-\alpha_L}\right\}.$$

Let $P_H > P_L$, then the probability of the joint-event is given as $\frac{P_L}{P_H} X_L^{-\alpha_L} < X_H^{-\alpha_H} \leq \frac{Q_L}{Q_H} X_L^{-\alpha_L}$. Then, the association probability of a T-UE in the decoupled-enabled region is

$$\begin{aligned}
&\mathbb{A}_D \\
&= \mathbb{P}\left\{X_H < \left(\frac{P_H}{P_L}\right)^{\frac{1}{\alpha_H}} X_L^{\frac{\alpha_L}{\alpha_H}}\right\} \\
&\quad - \mathbb{P}\left\{X_H < \left(\frac{Q_H}{Q_L}\right)^{\frac{1}{\alpha_H}} X_L^{\frac{\alpha_L}{\alpha_H}}\right\} \\
&\overset{a}{=} \int_0^\infty \left(1 - \exp\left\{-\pi\lambda_H \left(P_H/P_L\right)^{2/\alpha_H} x^{\frac{2\alpha_L}{\alpha_H}}\right\}\right. \\
&\quad \left. - \left(1 - \exp\left\{-\pi\lambda_H \left(Q_H/Q_L\right)^{2/\alpha_H} x^{\frac{2\alpha_L}{\alpha_H}}\right\}\right)\right) f_{X_L}(x)dx \\
&\overset{b}{=} 1 - 2\pi\lambda_L \\
&\quad \int_0^\infty \left(\frac{\alpha_H}{2\alpha_L} \mathcal{H}_{0,1}^{1,0}\left[\left(\sqrt{\pi\lambda_H}\right)^{\frac{\alpha_H}{\alpha_L}} \left(\frac{P_H}{P_L}\right)^{\frac{1}{\alpha_L}} x \middle| \begin{matrix}(-,-)\\ \left(0, \frac{\alpha_H}{2\alpha_L}\right)\end{matrix}\right]\right. \\
&\quad \left. \cdot \frac{1}{2}\mathcal{H}_{0,1}^{1,0}\left[\sqrt{\pi\lambda_L}x \middle| \begin{matrix}(-,-)\\ \left(0, \frac{1}{2}\right)\end{matrix}\right] x\right) dx - (1 - 2\pi\lambda_L \\
&\quad \int_0^\infty \left(\frac{\alpha_H}{2\alpha_L} \mathcal{H}_{0,1}^{1,0}\left[\left(\sqrt{\pi\lambda_H}\right)^{\frac{\alpha_H}{\alpha_L}} \left(\frac{Q_H}{Q_L}\right)^{\frac{1}{\alpha_L}} x \middle| \begin{matrix}(-,-)\\ \left(0, \frac{\alpha_H}{2\alpha_L}\right)\end{matrix}\right]\right. \\
&\quad \left. \cdot \frac{1}{2}\mathcal{H}_{0,1}^{1,0}\left[\sqrt{\pi\lambda_L}x \middle| \begin{matrix}(-,-)\\ \left(0, \frac{1}{2}\right)\end{matrix}\right] x\right) dx,
\end{aligned}$$

where $\overset{a}{=}$ is obtained by applying (18) and considering the association of the LAP with the T-UE as a first UL connection while, $\overset{b}{=}$ is obtained by exploiting Fox H-function given in (19), as shown at the bottom of the page, such that $m_1 = 1, n_1 = 0, v_1 = 0$, and $w_1 = 1$, and substituting (2.9.4) of [45]. In (19), $\Gamma(\mathfrak{t}) = \int_0^\infty \mathfrak{s}^{\mathfrak{t}-1} e^{-\mathfrak{s}} d\mathfrak{s}$ and γ is a non-zero complex-number. Moreover, $1 \leqslant m_1 \leqslant w_1, 0 \leqslant n_1 \leqslant v_1, A_\mathfrak{j} > 0, B_\mathfrak{j} > 0$, $\mathfrak{C}$ is a complex-contour, and $a_\mathfrak{j}, b_\mathfrak{j}$ are complex numbers. Finally, (3) is obtained by substituting (2.8.4) of [45].

APPENDIX B
DERIVATION OF (4)

For the T-UEs located in the decoupled-enabled regions, the LAP is associated with a T-UE in the first UL connection while the HAP is associated with a T-UE in the second UL connection. The PDF of the distance between the first UL connection of a T-UE and the serving LAP in the decoupled-enabled region is expressed in terms of complementary cumulative distribution function (CCDF), $F_{X_L}^{(c',D)}(.)$ as

$$f_{X_L}^{(UL1)}(x) = -\frac{d}{dx}\left(F_{X_L}^{(c',D)}(x)\right),$$

where in the superscript of $F_{X_L}^{(c',D)}(.)$, c' represents that it is a CCDF and D shows that the UEs in the decoupled-enabled region are considered. The CCDF of the distance between a T-UE and the serving LAP in the decoupled-enabled region

$$\mathcal{H}_{v_1,w_1}^{m_1,n_1}(\gamma) \triangleq \mathcal{H}_{v_1,w_1}^{m_1,n_1}\left[\gamma \middle| \begin{matrix}(a_1, A_1), \ldots, (a_{v_1}, A_{v_1})\\ (b_1, B_1), \ldots, (b_{w_1}, B_{w_1})\end{matrix}\right] = \frac{1}{2\pi\iota}\oint_{\mathfrak{C}} \frac{\Pi_{\mathfrak{j}=1}^{m_1}\Gamma(b_\mathfrak{j} + B_\mathfrak{j}\mathfrak{s})\Pi_{\mathfrak{j}=1}^{m_1}\Gamma(1 - a_\mathfrak{j} + A_\mathfrak{j}\mathfrak{s})}{\Pi_{\mathfrak{j}=n_1+1}^{v_1}\Gamma(a_\mathfrak{j} + A_\mathfrak{j}\mathfrak{s})\Pi_{\mathfrak{j}=m_1+1}^{w_1}\Gamma(1 - b_\mathfrak{j} + B_\mathfrak{j}\mathfrak{s})}\gamma^{-\mathfrak{s}} d\mathfrak{s}. \tag{19}$$

can be derived as [6]

$$F_{X_L}^{(c',D)}(x) = \mathbb{P}\left\{X_L > x \mid \frac{P_L}{P_H} X_L^{-\alpha_L} < X_H^{-\alpha_H} \leq \frac{Q_L}{Q_H} X_L^{-\alpha_L}\right\}$$
$$\stackrel{a}{=} \int_x^{\infty} \left(\exp\left\{ -\pi \lambda_H \left(\frac{Q_H}{Q_L}\right)^{\frac{2}{\alpha_H}} x^{\frac{2\alpha_L}{\alpha_H}} \right\} - \exp\left\{ -\pi \lambda_H \left(\frac{P_H}{P_L}\right)^{\frac{2}{\alpha_H}} x^{\frac{2\alpha_L}{\alpha_H}} \right\} \right) \frac{f_{X_L}(x)dx}{\mathbb{A}_D}, \quad (20)$$

where $\stackrel{a}{=}$ is obtained by applying Baye's rule and using (3) and (18).

APPENDIX C
DERIVATION OF (6)

In the decoupled access and RFA, the UL interference from outside of the HAP-region is derived as [7]

$$\mathcal{L}_{\mathcal{I}^{UL}_{\Phi_{L,A_H^O}}}(s) \stackrel{a}{=} \mathbb{E}_{\mathcal{I}^{UL}_{\Phi_{L,A_H^O}}, g_i}\left\{ \exp\left(-\frac{\tau x^{\alpha_L}}{Q_L} \sum_{i \in \Phi_{I_{L,A_H^O}}} Q_L g_i r_i^{-\alpha_L} \right) \right\}$$
$$\stackrel{b}{=} \mathbb{E}_{\mathcal{I}^{UL}_{\Phi_{L,A_H^O}}}\left\{ \prod_{i \in \Phi_{I_{L,A_H^O}}} \mathbb{E}_{g_i}\left\{ \exp\left(-x^{\alpha_L} g_i r_i^{-\alpha_L} \right) \right\} \right\}$$
$$\stackrel{c}{=} \mathbb{E}_{\mathcal{I}^{UL}_{\Phi_{L,A_H^O}}}\left\{ \prod_{i \in \Phi_{I_{L,A_H^O}}} \frac{1}{1 + \tau \left(\frac{r_i}{x}\right)^{-\alpha_L}} \right\}$$
$$\stackrel{d}{=} \exp\left\{ -2\pi \lambda_L \int_{r_1}^{r_2} \frac{r_i dr_i}{1 + \left(\frac{r_i}{\tau^{1/\alpha_L} x}\right)^{\alpha_L}} \right\}$$
$$\stackrel{e}{=} \exp\left\{ -\pi \lambda_L \tau^{2/\alpha_L} x^2 \int_{\left(\frac{r_1}{\tau^{1/\alpha_L} x}\right)^2}^{\left(\frac{r_2}{\tau^{1/\alpha_L} x}\right)^2} \frac{dw}{1 + w^{\alpha_L/2}} \right\},$$

where $\stackrel{a}{=}$ is obtained by substituting the value of $s = \frac{x\alpha_L}{Q_L}$, $\stackrel{b}{=}$ is obtained by mathematical-manipulations, $\stackrel{c}{=}$ is obtained by assuming the parameters of fading channel as m = 1 and $\Omega = 1$ for the NLoS communication, $\stackrel{d}{=}$ is obtained by using probability generating functional (PGFL) of an HPPP [32], where radius of $A_H^{\mathbf{O}}$ is r_1 and $A_H^{\mathbf{C}}$ is r_2, and $\stackrel{e}{=}$ follows by change of variables $w = \left(\frac{r_i}{\tau^{1/\alpha_L} x}\right)^2$. Finally, the UL interference at the LAP is obtained by performing the integration as in (6).

APPENDIX D
DERIVATION OF (10)

The UL interference of the MCP-distributed clustered WBJs at the serving UAV of the i-th tier is given in terms of the interference of the WBJs. Let $\upsilon(x) = \mathcal{L}_{\mathcal{I}_{\Phi_{J,i}}}(s)$ define the WBJ's interference at the UAV of tier i such that $s = \frac{x_i^{\alpha}\tau}{Q_i}$. Similar to [33], [48], the interference at the UAV of tier i is given by the conditional-PGFL, $\wp(\upsilon)$ and the PGFL, $\mathcal{G}(\upsilon)$ and is given as [7]

$$\wp(\upsilon) = \mathbb{E}\left\{\Pi_{x \in \Phi} \upsilon(x)\right\} = \mathcal{G}(\upsilon) \times \mho, \quad (21)$$

where

$$\mho \triangleq \exp\left\{ -\frac{P_j x^2 \tau^{2/\alpha_i} 2\pi \bar{c}}{Q_i \alpha_i r_j^2} \csc\left(\frac{2\pi}{\alpha_i}\right) \right\}. \quad (22)$$

For $\alpha_i > 2$, the PGFL can be solved. Thus, for the WBJs, $\mathcal{G}(\upsilon)$ is expressed as

$$\mathcal{G}(\upsilon) = \exp\left\{ -\lambda_j \pi \frac{P_j \tau^{2/\alpha_i} x^2}{Q_i} \int_0^{\infty} \left(1 - \exp\left\{\frac{-\bar{c}}{1+t^{\alpha_i/2}}\right\}\right) dt \right\}. \quad (23)$$

By substituting $\mho$ and $\mathcal{G}(\upsilon)$ in $\wp(\upsilon)$ and considering the ratio of the WBJ's transmit power to the UE's transmit power as $\Delta_i = \frac{P_j}{Q_i}$, the WBJ's interference is obtained in (10).

REFERENCES

[1] *IMT Traffic Estimates for the Years 2020 to 2030*, document Report ITU-R M. 2370–0, ITU-R Radiocommunication Sector of ITU, 2015.

[2] S. J. Nawaz, S. K. Sharma, S. Wyne, M. N. Patwary, and M. Asaduzzaman, "Quantum machine learning for 6G communication networks: State-of-the-art and vision for the future," *IEEE Access*, vol. 7, pp. 46317–46350, 2019.

[3] V. Sharma, M. Bennis, and R. Kumar, "UAV-assisted heterogeneous networks for capacity enhancement," *IEEE Commun. Lett.*, vol. 20, no. 6, pp. 1207–1210, Jun. 2016.

[4] E. Turgut and M. C. Gursoy, "Downlink analysis in unmanned aerial vehicle (UAV) assisted cellular networks with clustered users," *IEEE Access*, vol. 6, pp. 36313–36324, 2018.

[5] A. Fotouhi, H. Qiang, M. Ding, M. Hassan, L. G. Giordano, A. Garcia-Rodriguez, and J. Yuan, "Survey on UAV cellular communications: Practical aspects, standardization advancements, regulation, and security challenges," *IEEE Commun. Surveys Tuts.*, vol. 21, no. 4, pp. 3417–3442, 4th Quart., 2019.

[6] M. Arif, S. Wyne, K. Navaie, S. J. Nawaz, and S. H. Alvi, "Decoupled downlink and uplink access for aerial terrestrial heterogeneous cellular networks," *IEEE Access*, vol. 8, pp. 111172–111185, 2020.

[7] M. Arif, S. Wyne, K. Navaie, M. S. Haroon, and S. Qureshi, "Clustered jamming in aerial HetNets with decoupled access," *IEEE Access*, vol. 8, pp. 142218–142228, 2020.

[8] A. Al-Hourani, S. Kandeepan, and A. Jamalipour, "Modeling air-to-ground path loss for low altitude platforms in urban environments," in *Proc. IEEE Global Commun. Conf.*, Dec. 2014, pp. 2898–2904.

[9] A. Al-Hourani, S. Kandeepan, and S. Lardner, "Optimal LAP altitude for maximum coverage," *IEEE Wireless Commun. Lett.*, vol. 3, no. 6, pp. 569–572, Dec. 2014.

[10] S. Sekander, H. Tabassum, and E. Hossain, "Multi-tier drone architecture for 5G/B5G cellular networks: Challenges, trends, and prospects," *IEEE Commun. Mag.*, vol. 56, no. 3, pp. 96–103, Mar. 2018.

[11] M. Helmy and H. Arslan, "Utilization of aerial heterogeneous cellular networks: Signal-to-interference ratio analysis," *J. Commun. Netw.*, vol. 20, no. 5, pp. 484–495, Oct. 2018.

[12] Z. Li, Y. Wang, and Y. Liu, "Efficient resource allocation in UAV-BS dual connectivity heterogeneous networks," in *Proc. 9th Int. Conf. Inf. Sci. Technol. (ICIST)*, Aug. 2019, pp. 234–239.
[13] R. Amorim, I. Z. Kovacs, J. Wigard, G. Pocovi, T. B. Sorensen, and P. Mogensen, "Improving Drone's command and control link reliability through dual-network connectivity," in *Proc. IEEE 89th Veh. Technol. Conf. (VTC-Spring)*, Apr. 2019, pp. 1–6.
[14] X. Jia, Q. Fan, W. Xu, and L. Yang, "Cross-tier dual-connectivity designs of three-tier hetnets with decoupled uplink/downlink and global coverage performance evaluation," *IEEE Access*, vol. 7, pp. 16816–16836, 2019.
[15] M. Arif, S. Wyne, and J. Ahmed, "Efficiency analysis of a K-tier clustered HCN using dual connectivity with DUDe access," *AEU - Int. J. Electron. Commun.*, vol. 123, Aug. 2020, Art. no. 153291.
[16] M. G. Kibria, K. Nguyen, G. P. Villardi, W.-S. Liao, K. Ishizu, and F. Kojima, "A stochastic geometry analysis of multiconnectivity in heterogeneous wireless networks," *IEEE Trans. Veh. Technol.*, vol. 67, no. 10, pp. 9734–9746, Oct. 2018.
[17] M. N. Sial and J. Ahmed, "Analysis of K-tier 5G heterogeneous cellular network with dual-connectivity and uplink–downlink decoupled access," *Telecommun. Syst.*, vol. 67, no. 4, pp. 669–685, Apr. 2018.
[18] M. A. Lema, E. Pardo, O. Galinina, S. Andreev, and M. Dohler, "Flexible dual-connectivity spectrum aggregation for decoupled uplink and downlink access in 5G heterogeneous systems," *IEEE J. Sel. Areas Commun.*, vol. 34, no. 11, pp. 2851–2865, Nov. 2016.
[19] K. Smiljkovikj, P. Popovski, and L. Gavrilovska, "Analysis of the decoupled access for downlink and uplink in wireless heterogeneous networks," *IEEE Wireless Commun. Lett.*, vol. 4, no. 2, pp. 173–176, Apr. 2015.
[20] L. Zhang, W. Nie, G. Feng, F.-C. Zheng, and S. Qin, "Uplink performance improvement by decoupling uplink/downlink access in HetNets," *IEEE Trans. Veh. Technol.*, vol. 66, no. 8, pp. 6862–6876, Aug. 2017.
[21] M. Arif, S. Wyne, and J. Ahmed, "Performance analysis of downlink and uplink decoupled access in clustered heterogeneous cellular networks," *Telecommun. Syst.*, vol. 72, no. 3, pp. 355–364, Nov. 2019.
[22] F. Muhammad, Z. H. Abbas, G. Abbas, and L. Jiao, "Decoupled downlink-uplink coverage analysis with interference management for enriched heterogeneous cellular networks," *IEEE Access*, vol. 4, pp. 6250–6260, 2016.
[23] A. Ijaz, S. A. Hassan, S. A. R. Zaidi, D. N. K. Jayakody, and S. M. H. Zaidi, "Coverage and rate analysis for downlink HetNets using modified reverse frequency allocation scheme," *IEEE Access*, vol. 5, pp. 2489–2502, 2017.
[24] M. S. Haroon, F. Muhammad, Z. H. Abbas, G. Abbas, N. Ahmed, and S. Kim, "Proactive uplink interference management for nonuniform heterogeneous cellular networks," *IEEE Access*, vol. 8, pp. 55501–55512, 2020.
[25] F. Muhammad, M. S. Haroon, Z. H. Abbas, G. Abbas, and S. Kim, "Uplink interference management for hetnets stressed by clustered wideband jammers," *IEEE Access*, vol. 7, pp. 182679–182690, 2019.
[26] J. Miao and Z. Zheng, "Cooperative jamming for secure UAV-enabled mobile relay system," *IEEE Access*, vol. 8, pp. 48943–48957, 2020.
[27] Y. Wu, W. Fan, W. Yang, X. Sun, and X. Guan, "Robust trajectory and communication design for multi-UAV enabled wireless networks in the presence of jammers," *IEEE Access*, vol. 8, pp. 2893–2905, 2020.
[28] B. Duan, D. Yin, Y. Cong, H. Zhou, X. Xiang, and L. Shen, "Anti-jamming path planning for unmanned aerial vehicles with imperfect jammer information," in *Proc. IEEE Int. Conf. Robot. Biomimetics (ROBIO)*, Dec. 2018, pp. 729–735.
[29] M. S. Haroon, F. Muhammad, G. Abbas, Z. H. Abbas, A. K. Hassan, M. Waqas, and S. Kim, "Interference management in ultra-dense 5G networks with excessive drone usage," *IEEE Access*, vol. 8, pp. 102155–102164, 2020.
[30] K. Yoshikawa, K. Yamamoto, T. Nishio, and M. Morikura, "Grid-based exclusive region design for 3D UAV networks: A stochastic geometry approach," *IEEE Access*, vol. 7, pp. 103806–103814, 2019.
[31] Y. Sun, T. Wang, and S. Wang, "Location optimization and user association for unmanned aerial vehicles assisted mobile networks," *IEEE Trans. Veh. Technol.*, vol. 68, no. 10, pp. 10056–10065, Oct. 2019.
[32] S. N. Chiu, D. Stoyan, W. S. Kendall, and J. Mecke, *Stochastic Geometry and its Applications*. Hoboken, NJ, USA: Wiley, 2013.
[33] R. K. Ganti and M. Haenggi, "Interference and outage in clustered wireless ad hoc networks," *IEEE Trans. Inf. Theory*, vol. 55, no. 9, pp. 4067–4086, Sep. 2009.
[34] K. Grover, A. Lim, and Q. Yang, "Jamming and anti–jamming techniques in wireless networks: A survey," *Int. J. Ad Hoc Ubiquitous Comput.*, vol. 17, no. 4, pp. 197–215, 2014.
[35] W. Xu, W. Trappe, Y. Zhang, and T. Wood, "The feasibility of launching and detecting jamming attacks in wireless networks," in *Proc. 6th ACM Int. Symp. Mobile ad Hoc Netw. Comput. - MobiHoc*, 2005, pp. 46–57.
[36] P. Tague, D. Slater, R. Poovendran, and G. Noubir, "Linear programming models for jamming attacks on network traffic flows," in *Proc. 6th Intl Symp. Model. Optim.*, Apr. 2008, pp. 207–216.
[37] K. Pelechrinis, M. Iliofotou, and S. V. Krishnamurthy, "Denial of service attacks in wireless networks: The case of jammers," *IEEE Commun. Surveys Tuts.*, vol. 13, no. 2, pp. 245–257, 2nd Quart., 2011.
[38] P. S. Bithas, V. Nikolaidis, A. G. Kanatas, and G. K. Karagiannidis, "UAV-to-Ground communications: Channel modeling and UAV selection," *IEEE Trans. Commun.*, vol. 68, no. 8, pp. 5135–5144, Aug. 2020.
[39] L. C. Andrews and L. C. Andrews, *Special Functions of Mathematics for Engineers*. New York, NY, USA: McGraw-Hill, 1992.
[40] Z. H. Abbas, M. S. Haroon, G. Abbas, and F. Muhammad, "SIR analysis for non-uniform HetNets with joint decoupled association and interference management," *Comput. Commun.*, vol. 155, pp. 48–57, Apr. 2020.
[41] M. S. Haroon, Z. H. Abbas, G. Abbas, and F. Muhammad, "Coverage analysis of ultra-dense heterogeneous cellular networks with interference management," *Wireless Netw.*, vol. 26, no. 3, pp. 2013–2025, Apr. 2020.
[42] T. D. Novlan, H. S. Dhillon, and J. G. Andrews, "Analytical modeling of uplink cellular networks," *IEEE Trans. Wireless Commun.*, vol. 12, no. 6, pp. 2669–2679, Jun. 2013.
[43] Z. Sattar, J. V. C. Evangelista, G. Kaddoum, and N. Batani, "Spectral efficiency analysis of the decoupled access for downlink and uplink in two-tier network," *IEEE Trans. Veh. Technol.*, vol. 68, no. 5, pp. 4871–4883, May 2019.
[44] K. Smiljkovikj, H. Elshaer, P. Popovski, F. Boccardi, M. Dohler, L. Gavrilovska, and R. Irmer, "Capacity analysis of decoupled downlink and uplink access in 5G heterogeneous systems," 2014, *arXiv:1410.7270*. [Online]. Available: http://arxiv.org/abs/1410.7270
[45] A. A. Kilbas, *H-Transforms: Theory and Applications*. Boca Raton, FL, USA: CRC Press, 2004.
[46] K. Smiljkovikj, L. Gavrilovska, and P. Popovski, "Efficiency analysis of downlink and uplink decoupling in heterogeneous networks," in *Proc. IEEE Int. Conf. Commun. Workshop (ICCW)*, Jun. 2015, pp. 125–130.
[47] J. G. Andrews, A. K. Gupta, and H. S. Dhillon, "A primer on cellular network analysis using stochastic geometry," 2016, *arXiv:1604.03183*. [Online]. Available: http://arxiv.org/abs/1604.03183
[48] Y. Wang and Q. Zhu, "Modeling and analysis of small cells based on clustered stochastic geometry," *IEEE Commun. Lett.*, vol. 21, no. 3, pp. 576–579, Mar. 2017.

MOHAMMAD ARIF received the B.S. degree in electrical engineering from the University of Engineering and Technology, Peshawar, Pakistan, in 2012, and the M.S. degree in electrical engineering from the COMSATS University Islamabad (CUI), Islamabad, Pakistan, in 2014, where he is currently pursuing the Ph.D. degree with the Department of Electrical and Computer Engineering.

His research interests include aerial and terrestrial heterogeneous cellular networks, dual connectivity, uplink and downlink interference management, reverse frequency allocation, indoor localization, signal processing, and channel coding.

SHURJEEL WYNE (Senior Member, IEEE) received the Ph.D. degree from Lund University, Sweden, in 2009.

From 2009 to 2010, he was a Postdoctoral Research Fellow, funded by the High-Speed Wireless Center, Lund University. Since 2010, he has been with the Department of Electrical and Computer Engineering, COMSATS University Islamabad (CUI), Islamabad, Pakistan, where he is currently an Associate Professor. His research interests include wireless channel characterization, multi-antenna systems, cooperative communications, physical layer security, and vehicular communications. He was a co-recipient of the Best Paper Award of the Antennas and Propagation Track at the IEEE VTC2013-Spring.

KEIVAN NAVAIE (Senior Member, IEEE) is currently with the School of Computing and Communications, Lancaster University, U.K. His research interests include provisioning dependable connectivity and positioning to intelligent cyber-physical systems. He is a Fellow of the IET, a Senior Fellow of the HEA, and a Chartered Engineer in the U.K. He currently serves on the Editorial Board of the IEEE TRANSACTIONS ON WIRELESS COMMUNICATIONS, IEEE COMMUNICATIONS LETTERS, and IEEE COMMUNICATIONS SURVEYS AND TUTORIAL.

MUHAMMAD SAJID HAROON (Graduate Student Member, IEEE) received the B.Sc. degree in electronics engineering from International Islamic University Islamabad, Pakistan, in 2007, the M.S. degrees in electrical engineering from the COMSATS Institute of Information Technology, Attock, Pakistan, in 2013, and the Ph.D. degree from the Ghulam Ishaq Khan Institute of Engineering Science and Technology, Swabi, Pakistan, in 2020, with a focus on interference management in next-generation cellular networks using tools from stochastic geometry.

SADIA QURESHI received the M.S. degree in electrical engineering from the University of Engineering and Technology, Peshawar, Pakistan. She is currently pursuing the Ph.D. degree with the University of Technology, Sydney. She is also a full-time Research Scholar with the School of Electrical and Data Engineering, University of Technology, Sydney. Her research interests include heterogeneous networks, signal processing, wireless sensor networks, software-defined networking, and optical networks.